DALTON
FULL PAPER

Stereochemical effects on the spin-state transition shown by salts of $[FeL_2]^{2+}$ [L = 2,6-di(pyrazol-1-yl)pyridine]

Joanne M. Holland,[a] Judith A. McAllister,[b,c] Colin A. Kilner,[a] Mark Thornton-Pett,[a] Adam J. Bridgeman *[d] and Malcolm A. Halcrow *[a]

[a] *School of Chemistry, University of Leeds, Woodhouse Lane, Leeds, UK LS2 9JT.*
E-mail: M.A.Halcrow@chem.leeds.ac.uk
[b] *Department of Chemistry, University of Cambridge, Lensfield Road, Cambridge, UK CB2 1EW*
[c] *Interdisciplinary Research Centre in Superconductivity, University of Cambridge, Madingley Road, Cambridge, UK CB3 0HE*
[d] *Department of Chemistry, University of Hull, Kingston-Upon-Hull, UK HU6 7RX.*
E-mail: A.J.Bridgeman@hull.ac.uk

Received 18th September 2001, Accepted 15th November 2001
First published as an Advance Article on the web 28th January 2002

The syntheses of $[Fe(L^1H)_2]X_2$ (L^1H = 2,6-di(pyrazol-1-yl)pyridine [L^1H]; X^- = BF_4^-, PF_6^-) are described. Solvent-free $[Fe(L^1H)_2][BF_4]_2$ shows an approximately D_{2d}-symmetric metal centre in the crystal, and undergoes an unusual abrupt spin-state transition centered at 261 K in the solid, or at 248 K in acetone solution. A solvated phase $[Fe(L^1H)_2][BF_4]_2\cdot2.9CH_3NO_2\cdot0.25H_2O$ can be grown at 240 K, which undergoes an irreversible spin-state transition between 260 and 265 K. In contrast, solid $[Fe(L^1H)_2][PF_6]_2$ adopts an unusual C_2-symmetric coordination geometry, reflecting a *ca.* 28° twist of one L^1H ligand with respect to each other. This salt is high-spin in the range 10–330 K. DFT calculations have rationalised this unusual structure as a Jahn–Teller distortion of the ^5E ground state of the six-coordinate Fe(II) ion. This distortion is favoured by the restricted bite-angle of the L^1H ligands.

We have recently described that substitution at the 3- and 3''-positions of the 2,6-di(pyrazol-1-yl)pyridine skeleton leads to a change in electronic ground state for $[Cu(L^1R)_2]^{2+}$, from the usual $\{d_{x^2-y^2}\}^1$ ground state when R = H to $\{d_{z^2}\}^1$ when R = Pr^i, Ph or Mes (Mes = mesityl).[1–4] We were interested to extend these studies to other metal ions,[5] and particularly to $[Fe(L^1R)_2]^{2+}$ complexes, to examine how the L^1R substituents perturb the spin-cross-over behaviour exhibited by many $[FeL_2]^{2+}$ complexes, where L is a meridional tris-imine.[6,7] We noted in particular that salts of $[Fe(L^2)_2]^{2+}$ [L^2 = 2,6-di(pyrazol-3-yl)pyridine, a structural isomer of L^1H] can be isolated in both high-spin or low-spin forms, depending on the anion employed and/or the degree of hydration in the solid.[8,9] Many of these salts exhibit both thermally-, pressure- or light-induced spin-crossover transitions, whose physics has been extensively studied.[9,10]

We have previously communicated that $[Fe(L^1H)_2][BF_4]_2$ undergoes an abrupt spin-state transition at 261 K, exhibiting a small hysteresis loop.[11] We now present a more detailed study of the chemistry of $[Fe(L^1H)_2]^{2+}$. A report of the synthesis, room-temperature solution magnetic moment and voltammetry of $[Fe(L^1H)_2][PF_6]_2$ (**1[PF₆]₂**) appeared during the course of this work.[12]

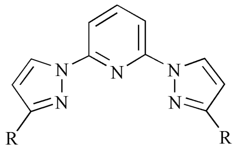

L^1R
(R = H, Pr^i, Ph, Mes)

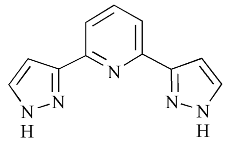

L^2

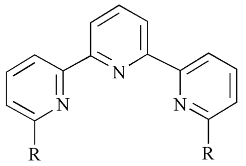

L^3R
(R = H, Me, Ph)

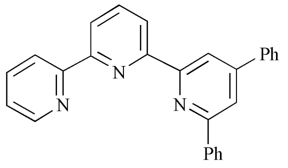

L^4

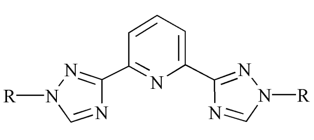

L^5R
(R = H, Me)

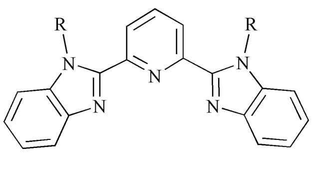

L^6R
(R = H, Me)

Results and discussion

Syntheses and magnetochemical characterisation of $[Fe(L^1H)_2]^{2+}$ salts

Complexation of $Fe[BF_4]_2\cdot6H_2O$ by 2 molar equivalents of L^1H[13] in warm acetone affords a brown solution. Filtration and concentration of this solution yields $[Fe(L^1H)_2][BF_4]_2$ (**1[BF₄]₂**) as a mustard-coloured microcrystalline solid. Reaction of $FeCl_2\cdot6H_2O$ with 2 molar equivalents of L^1H in refluxing MeOH again affords a brown solution. Addition of 2.2 molar equivalents of NH_4PF_6 gives a bright yellow microcrystalline precipitate of $[Fe(L^1H)_2][PF_6]_2$ (**1[PF₆]₂**).

For powdered **1[BF₄]₂**, the $\chi_M T$ *vs.* T curve shows an abrupt transition centred at 259 K, from a high-spin state at higher temperature ($\chi_M T$ = 3.6–3.7 cm^3 K mol^{-1} [14]) to a low-spin state ($\chi_M T \leq 0.3$ cm^3 K mol^{-1} [14]); Fig. 1.[11] This transition has a width

DOI: 10.1039/b108468m

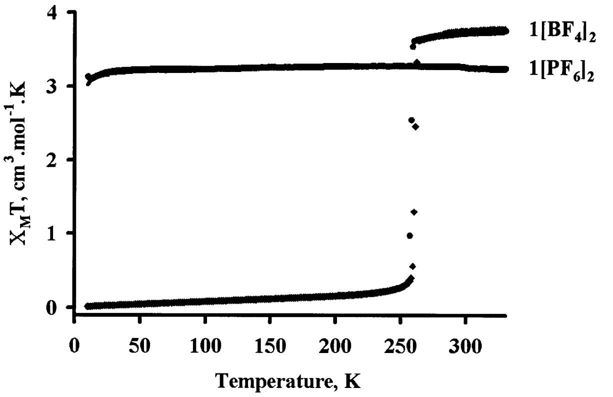

Fig. 1 Plots of χ_MT *vs.* T for polycrystalline **1[BF$_4$]$_2$** and **1[PF$_6$]$_2$**. Data for **1[BF$_4$]$_2$** are shown in both cooling (●) and warming (◆) modes. The solid line through the **1[PF$_6$]$_2$** data shows the fit to the zero-field splitting Hamiltonian; details are given in the text.

of 3 K and a 3 K hysteresis loop. In contrast, χ_MT for powdered **1[PF$_6$]$_2$** is constant at 3.2–3.3 cm^3 K mol^{-1}, before decreasing slightly below 25 K (Fig. 1). This implies that this compound is high-spin over the complete temperature range, with an $S = 2$ quintet ground state that shows zero-field splitting at low temperature. Fitting of these data to the appropriate spin-Hamiltonian[14] afforded values of $g = 2.09$ and $D = 4.9$ cm^{-1}.

The ^{1}H NMR spectrum of **1[BF$_4$]$_2$** in CD$_3$CN is broadened and contact shifted, and displays the number of resonances expected from a single C_2- or *m*-symmetric L^{1}H environment. Unfortunately, with the exception of the pyridine H^4 protons which resonate at 2.6 ppm, it is impossible to assign each resonance definitively from the L^{1}H backbone. However, these spectra clearly demonstrate that the Fe(II) centres in solutions of **1[BF$_4$]$_2$** are paramagnetic, and so predominantly high-spin. The ^{1}H NMR spectra of this complex in CD$_3$NO$_2$ and {CD$_3$}$_3$CO showed the same number of peaks as in CD$_3$CN, with chemical shifts that varied by <3 ppm between solvents. This shows that the [Fe(L^{1}H)$_2$]$^{2+}$ dication does not undergo solvolysis upon dissolution, and that its magnetic structures in these three solvents are the same.

Variable temperature magnetic susceptibilities of **1[BF$_4$]$_2$** were determined in 99 : 1 {CD$_3$}$_3$CO : Si(CH$_3$)$_4$. χ_MT for **1[BF$_4$]$_2$** decreases steadily upon cooling, from 3.7 cm^3 mol^{-1} K at 325 K to 0.2 cm^3 mol^{-1} K at 185 K [Fig. 2(a)]. This demonstrates that the compound undergoes an almost complete spin-state transition over this temperature range, centred at 248(1) K. Since the L^{1}H ligands do not dissociate significantly in solution, the shift of this equilibrium to lower temperature in solution compared with the solid state must reflect changes in the intermolecular interactions in these two phases.[15] A van't Hoff analysis[16] of this equilibrium afforded ΔH = 24.1(2) kJ mol^{-1} [Fig. 2(b)], leading to ΔS = 101(1) J mol^{-1} K^{-1}.† These are both higher than the values of ΔH = 17.2(2) kJ mol^{-1} and ΔS = 66.2(8) J mol^{-1} K^{-1} exhibited by this transition in the solid state.[11]

The UV/vis/NIR spectra of **1[BF$_4$]$_2$** in MeCN at 298 K show a weak near-IR absorption envelope centred at $\nu_{max} = 10.4 \times 10^3$ cm^{-1} (ε_{max} = 8.4 M^{-1} cm^{-1}), that can be assigned to a spin-allowed $^5T_{2g} \longrightarrow {}^5E_g$ transition of an $S = 2$ Fe(II) ion in O_h notation.[17] This band is clearly split into two components, which can be attributed to splitting of the pseudo-Jahn–Teller-active ^5E_g excited state.[17] The spectrum also contains two MLCT transitions lying in the range ν_{max} = 23.9 and 26.3 × 10^3 cm^{-1} (ε_{max} = 1400 M^{-1} cm^{-1}). These three spectra closely resemble that of solid [Fe(L^2)$_2$][BF$_4$]$_2$ in its high-spin state,[8] and support the NMR data in showing that **1[BF$_4$]$_2$** is completely high-spin in solution at 298 K. These d–d bands discussed below occur at essentially identical energies in MeNO$_2$, again demonstrating that the complex does not undergo solvolysis upon dissolution. In addition to the peaks discussed below, the spectra contain intense ligand-based $\pi \longrightarrow \pi^*$ transitions in the UV region.

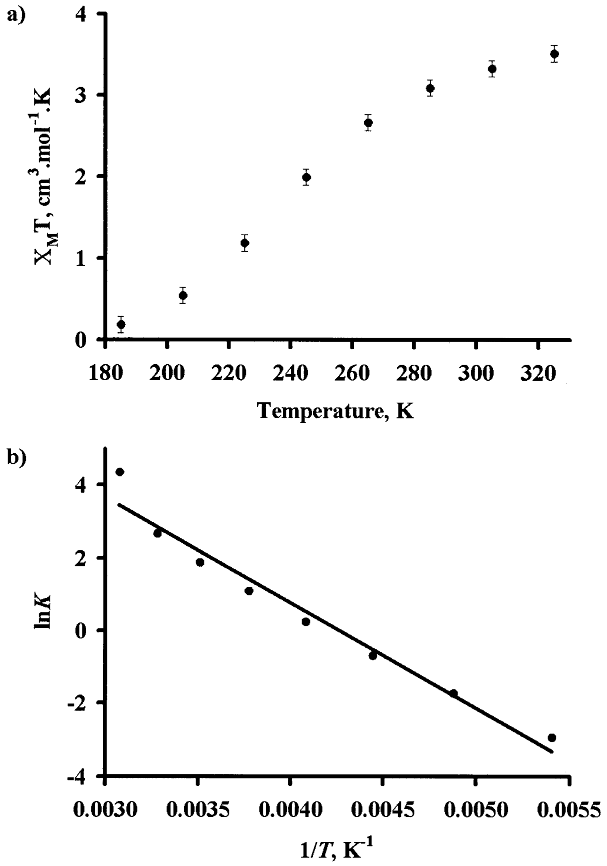

Fig. 2 (a) Plot of χ_MT *vs.* T for **1[BF$_4$]$_2$** in 99 : 1 {CD$_3$}$_3$CO : Si(CH$_3$)$_4$. (b) van't Hoff plot of the spin-state equilibrium for **1[BF$_4$]$_2$** from the data in Fig. 2(a), showing the line of best fit.

Crystallography

Vapour diffusion of Et$_2$O into solutions of **1[BF$_4$]$_2$** in acetone, MeNO$_2$ or MeCN at 290 K affords isomorphous, air-stable crystals which do not contain solvent by microanalysis. These crystals undergo a sharp colour change from yellow to dark brown at 261 ± 1 K, corresponding to the spin-state transition exhibited by this compound (Fig. 1). The temperature of this transition was confirmed by determining the crystallographic unit cell between 240 and 300 K, which demonstrated an abrupt discontinuity within the range 259–261 K in both cooling and warming modes (Fig. 3). This transition does not involve a change in space group, but is characterised by a decrease of 0.55 Å in the crystallographic *c*-direction, an increase of 0.05 Å in *b*, and an increase of 2.0° in β as the temperature is lowered. The decrease in unit cell volume associated with the phase transition (ignoring thermal contraction effects) is 35 ± 5 Å^3 or 2.6%, which is a typical value for a spin-state transition in an Fe(II) complex.[18–20] The mosaicity of the crystal increases sharply below the transition temperature, which leads to greatly increased esds on the cell parameters and can be attributed to increased lattice strain associated with the changing unit cell volume. This problem is alleviated upon further cooling of the crystal.

As we have previously described,[11] the [Fe(L^{1}H)$_2$]$^{2+}$ dications in crystalline **1[BF$_4$]$_2$** have approximate local D_{2d} symmetry (Fig. 4). The Fe–N bond lengths in the crystal at 290 K are consistent with a high-spin Fe(II) ion, lying within the range

---

† The deviation of the experimental data in Fig. 2(b) from linearity arises because ΔH varies slightly with temperature.[16] Hence, ΔH and ΔS derived by this analysis correspond to average values over the wide temperature range of the experiment.

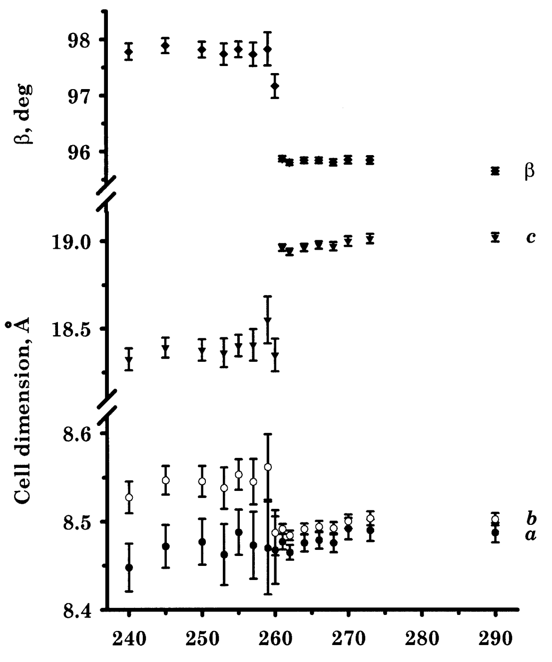

Fig. 3 Plot of the variation of the unit cell parameters of **1[BF$_4$]$_2$** with temperature.

2.1248(19)–2.185(3) Å. In contrast, at 240 K the Fe–N bond lengths have shortened to 1.893(3)–1.981(4) Å, and are characteristic of a low-spin Fe(II) centre.[11] The difference between the average Fe–N distances at 290 and 240 K in **1[BF$_4$]$_2$** is 0.215(10) Å, which is a typical value for a spin-state transition involving an Fe(II) complex with a hexa-nitrogen donor set.[6,7]

The relative ligand field strengths at the Fe ion in the high- and low-spin forms of **1[BF$_4$]$_2$** can be estimated from the crystallographic data using eqn. (1), where r_{HS} and r_{LS} are,

$$\frac{10Dq^{\mathrm{LS}}}{10Dq^{\mathrm{HS}}} = \left(\frac{r_{\mathrm{HS}}}{r_{\mathrm{LS}}}\right)^{6} \tag{1}$$

respectively, the average Fe–N bond lengths in the high-spin and low-spin forms of the complex.[7]

From the X-ray data at 290 and 240 K, this equation gives a ratio of 1.87(1) for **1[BF$_4$]$_2$**, which is substantially greater than the value of 1.74 that is typically observed for spin-crossover compounds.[7] Discrepancies from this formula can arise if a sample contains mixtures of high- and low-spin Fe ions at the temperatures examined.[21] This cannot be true here, since the magnetic measurements described above demonstrate that at both temperatures essentially all Fe ions in the sample will be in the same spin-state.[11] We therefore suggest that this anomalous ratio might reflect the strongly axial nature of the coordination sphere in this complex, so that that the averaged Fe–N bond lengths do not provide an accurate description of $10Dq$.

Dark brown crystals of **1[BF$_4$]$_2$** can also be grown from MeCN/Et$_2$O at 240 K (*i.e.* below the spin-crossover temperature). These low-temperature crystals are isomorphous with those grown at 290 K, and also undergo the same spin-state transition upon warming to 260 ± 1 K. Unexpectedly, however, vapor diffusion of Et$_2$O into MeNO$_2$ solutions of the complex at 240 K afforded a new solvated phase of this material, of formula **1[BF$_4$]$_2$**·2.9CH$_3$NO$_2$·0.25H$_2$O. A structure determination of this new polymorph revealed two independent complex cations in the asymmetric unit, both containing low-spin Fe(II) centres with metric parameters that closely resemble those of the low-spin unsolvated phase of **1[BF$_4$]$_2$** (Table 1).[11] While one of these (molecule 2 in Table 1) has almost perfect D_{2d} symmetry within experimental error, one L^{1}H ligand in the other molecule (molecule 1) is coordinated asymmetrically, the bond Fe(1)–N(25) being 0.040(4) Å longer than Fe(1)–N(30) (Table 1, Fig. 4).

Interestingly, dark brown crystals of this low-temperature solvate that are encapsulated in mineral oil decompose to a yellow powder upon warming over the range 260–265 K, consistent with a spin-state transition that involves a change in space group. That two different polymorphs of **1[BF$_4$]$_2$** should undergo spin-crossover at virtually the same temperature is unexpected, in that it is well known that the degree of solvation,[7] or simply the intermolecular packing,[22] within a crystal can have a profound effect on its spin-crossover properties. We suggest that these results imply that, in the absence of any strongly directional intermolecular hydrogen-bonding or π–π interactions, the magnetic behaviour of **1[BF$_4$]$_2$** is governed primarily by the electrostatic interaction between the anions and cations. Since the distance between neighbouring cations and anions in a molecular crystal will be similar in the presence or absence of lattice solvent, the thermodynamics of the spin-state transition of **1[BF$_4$]$_2$** would then be almost identical for both polymorphs of this material, as is observed.

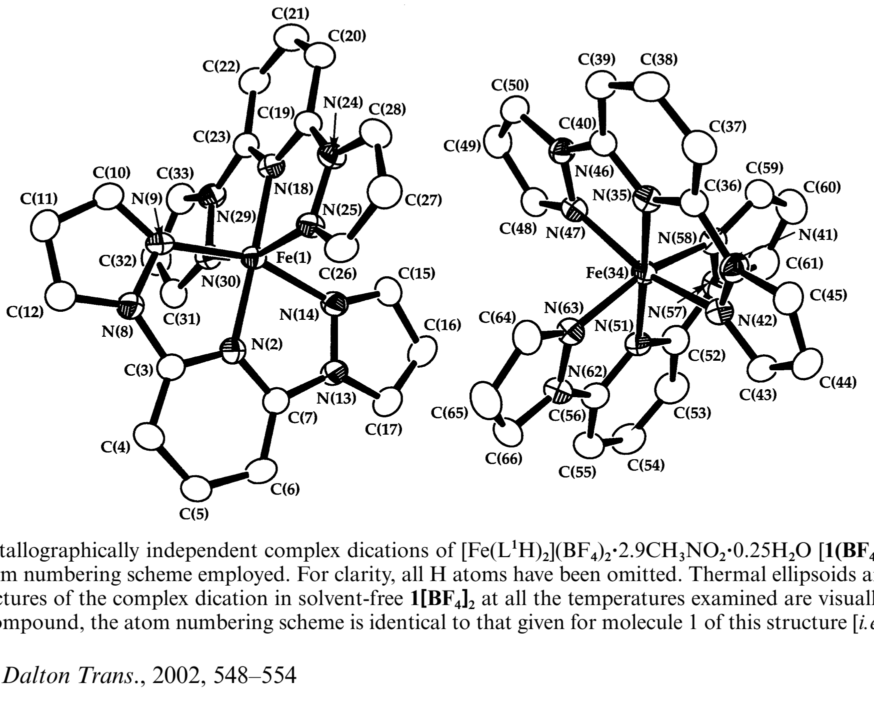

Fig. 4 Views of the crystallographically independent complex dications of [Fe(L^{1}H)$_2$](BF$_4$)$_2$·2.9CH$_3$NO$_2$·0.25H$_2$O [**1**(**BF$_4$**)$_2$·2.9CH$_3$NO$_2$·0.25H$_2$O] at 150 K, showing the atom numbering scheme employed. For clarity, all H atoms have been omitted. Thermal ellipsoids are at the 50% probability level. The molecular structures of the complex dication in solvent-free **1[BF$_4$]$_2$** at all the temperatures examined are visually indistinguishable from those here. In the latter compound, the atom numbering scheme is identical to that given for molecule 1 of this structure [*i.e.* Fe(1)–C(33)].

Table 1 Selected bond lengths (Å) and angles (°) in the single crystal X-ray structure of $[Fe(L^1H)_2](BF_4)_2 \cdot 2.9CH_3NO_2 \cdot 0.25H_2O$ [$\mathbf{1(BF_4)_2} \cdot 2.9CH_3NO_2 \cdot 0.25H_2O$]

Molecule 1		Molecule 2	
Fe(1)–N(2)	1.902(3)	Fe(34)–N(35)	1.899(3)
Fe(1)–N(9)	1.975(3)	Fe(34)–N(42)	1.977(3)
Fe(1)–N(14)	1.972(3)	Fe(34)–N(47)	1.974(3)
Fe(1)–N(18)	1.903(3)	Fe(34)–N(51)	1.903(3)
Fe(1)–N(25)	1.991(3)	Fe(34)–N(58)	1.983(3)
Fe(1)–N(30)	1.951(3)	Fe(34)–N(63)	1.976(3)
N(2)–Fe(1)–N(9)	80.40(12)	N(35)–Fe(34)–N(42)	80.35(12)
N(2)–Fe(1)–N(14)	79.95(12)	N(35)–Fe(34)–N(47)	79.91(12)
N(2)–Fe(1)–N(18)	178.26(13)	N(35)–Fe(34)–N(51)	177.53(13)
N(2)–Fe(1)–N(25)	101.40(12)	N(35)–Fe(34)–N(58)	102.40(13)
N(2)–Fe(1)–N(30)	98.27(12)	N(35)–Fe(34)–N(63)	97.69(13)
N(9)–Fe(1)–N(14)	160.13(12)	N(42)–Fe(34)–N(47)	160.24(12)
N(9)–Fe(1)–N(18)	98.47(12)	N(42)–Fe(34)–N(51)	99.64(13)
N(9)–Fe(1)–N(25)	95.55(12)	N(42)–Fe(34)–N(58)	91.79(12)
N(9)–Fe(1)–N(30)	88.08(12)	N(42)–Fe(34)–N(63)	91.18(12)
N(14)–Fe(1)–N(18)	101.11(12)	N(47)–Fe(34)–N(51)	100.12(12)
N(14)–Fe(1)–N(25)	91.15(12)	N(47)–Fe(34)–N(58)	91.64(12)
N(14)–Fe(1)–N(30)	91.88(12)	N(47)–Fe(34)–N(63)	92.25(12)
N(18)–Fe(1)–N(25)	80.00(12)	N(51)–Fe(34)–N(58)	80.07(13)
N(18)–Fe(1)–N(30)	80.35(12)	N(51)–Fe(34)–N(63)	79.85(13)
N(25)–Fe(1)–N(30)	160.33(12)	N(58)–Fe(34)–N(63)	159.91(13)

Table 2 Selected bond lengths (Å) and angles (°) in the single crystal X-ray structures of $[Fe(L^1H)_2](PF_6)_2$ [$\mathbf{1[PF_6]_2}$]. Primed atoms are related to unprimed atoms by the relation $1 - x, y, 1/2 - z$

Fe(1)–N(2)	2.1723(13)
Fe(1)–N(9)	2.1987(14)
Fe(1)–N(14)	2.2182(14)
N(2)–Fe(1)–N(2′)	154.18(7)
N(2)–Fe(1)–N(9)	72.00(5)
N(2)–Fe(1)–N(9′)	129.52(5)
N(2)–Fe(1)–N(14)	71.76(5)
N(2)–Fe(1)–N(14′)	89.08(5)
N(9)–Fe(1)–N(9′)	85.80(7)
N(9)–Fe(1)–N(14)	141.31(5)
N(9)–Fe(1)–N(14′)	107.38(5)
N(14)–Fe(1)–N(14′)	85.10(7)

A single crystal X-ray analysis of $\mathbf{1[PF_6]_2}$ was undertaken at 120 K. The asymmetric unit of this compound contains half a complex cation with Fe(1) lying on a crystallographic C_2 axis, and one PF_6^- anion. The Fe(1)–N bond lengths are typical of a high-spin Fe(II) centre (Table 2, Fig. 5).[6,7] However, in contrast to $\mathbf{1[BF_4]_2}$, the Fe(1) atom in $\mathbf{1[PF_6]_2}$ is strongly distorted away from a D_{2d} structure. This difference is manifest most obviously in the '*trans*' angle N(2)–Fe(1)–N(2′) = 154.18(7)°, and in the dihedral angle of 62.64(1)° between the least-squares planes of the two ligands in the cation. This unusual coordination geometry is similar to those exhibited by high-spin $[Fe(L^3Ph)_2][ClO_4]_2$ and $[Fe(L^4)_2][ClO_4]_2$ in the crystal,[23] but has not been observed otherwise in Fe(II)/tris-imine chemistry.

Calculations

Density functional (DF) and cellular ligand field (CLF) calculations were carried out using the crystal structure coordinates of $\mathbf{1[BF_4]_2}$ at 290 and 150 K, and of $\mathbf{1[PF_6]_2}$ at 150 K. The DF calculations demonstrate the following ordering of electronic stability in the gas phase at 0 K (Table 3):

$$\text{Low-spin} > \text{High-spin } (C_2) > \text{High-spin } (D_{2d})$$

This ordering cannot be used to predict the relative energies of the spin-states of $\mathbf{1}^{2+}$ in condensed media, however, since these will also depend on their vibrational energies and, possibly, on intermolecular interactions,[24,25] both of which were not included in this study. The higher Lewis acidity of low-spin Fe(II) is demonstrated by the Mulliken charge at Fe (Table 3). This is effectively zero for the low-spin complex but *ca.* +0.6 for the high-spin forms. The bond lengths are much shorter, and the Fe–N bond orders considerably larger, in the low-spin form. This demonstrates the antibonding character of the octahedral e_g orbitals, which are both half-occupied in high-spin $\mathbf{1}^{2+}$ (Table 3). The Fe–N{pyridine} bond orders are smaller than those for the Fe–N{pyrazole} bonds (Table 3), as the shorter bonds increase this antibonding interaction.

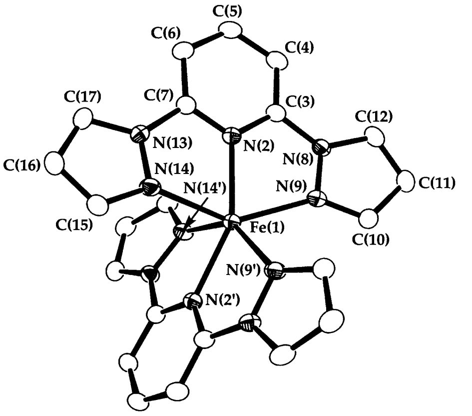

Fig. 5 View of the complex dication in the structure of $[Fe(L^1H)_2][PF_6]_2$ [$\mathbf{1[PF_6]_2}$], showing the atom numbering scheme employed. The molecule lies on a crystallographic C_2 axis passing through Fe(1). For clarity, all H atoms have been omitted. Thermal ellipsoids are at the 50% probability level.

In all three species, the shorter axial Fe–N{pyridine} bonds lead to splitting of the octahedral e_g levels, into a_1 (d_{z^2}) > b_1 ($d_{x^2-y^2}$). The octahedral t_{2g} levels are also antibonding, owing to the π-donor nature of the L^1H ligand.[2] In D_{2d} symmetry, these orbitals split into e (d_{xz}, d_{yz}) + b_2 (d_{xy}) because of two perturbations. Firstly, L^1H is only a π-donor perpendicular to the ligand plane. With an octahedral ligand bite angle ($\alpha = 90°$, Scheme 1), the b_2 orbital interacts with the p_π orbitals of the four pyrazole groups and the e-orbitals interact with one pyridine p_π function. In the CLF model, the antibonding shifts are:

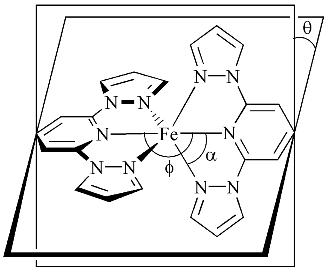

Scheme 1 Angles referred to in the discussion of the Jahn–Teller distortion in high-spin $[Fe(L^1H)_2]^{2+}$.

$$\varepsilon\,(d_{xz}, d_{yz}) = e_\pi \text{ (pyridine)}$$
$$\varepsilon\,(d_{xy}) = 4e_\pi \text{ (pyrazole)}$$

Hence, relative energies of b_2 > e might be expected unless the two types of base are very different. Secondly, the stiffness of the L^1H ligand results in ligand bite angles of <90° ($\alpha \approx 73°$, Scheme 1). This leads to an antibonding interaction between the pyrazole lone pairs and the d_{xz} and d_{yz} orbitals. On a σ-only or crystal-field model, e > b_2 is expected from this second distortion. The DF calculations on all three compounds give e > b_2, due to the balance of these effects.

Hence, the ground configuration of the high-spin (D_{2d}) form is $(e)^3(b_2)^1(b_1)^1(a_1)^1$, affording a Jahn–Teller-unstable ^5E ground term. This is analogous to the $^5T_{2g}$ ground term shown by high-spin, strictly octahedral Fe(II) complexes. These latter do not commonly exhibit large Jahn–Teller distortions, however,

Table 3 Calculated bond orders, Mulliken charges, energies and magnetic properties for the three forms of $[Fe(L^1H)_2]^{2+}$. The atom numbering scheme is the same as that used for the crystal structures of these compounds in this work or in ref. 11, while the bond lengths are taken from X-ray crystallographic data

	Low-spin (D_{2d})	High-spin (D_{2d})	High-spin (C_2)
Bond length/Å (bond order)			
Fe(1)–N(2){pyridine}	1.900 (0.53)	2.128 (0.22)	2.172 (0.27)
Fe(1)–N(9){pyrazole}	1.986 (0.56)	2.202 (0.37)	2.199 (0.31)
Fe(1)–N(14){pyrazole}	1.968 (0.57)	2.181 (0.38)	2.218 (0.42)
Fe(1)–N(18){pyridine}	1.902 (0.53)	2.130 (0.21)	2.172 (0.27)
Fe(1)–N(25){pyrazole}	1.989 (0.56)	2.191 (0.37)	2.199 (0.31)
Fe(1)–N(30){pyrazole}	1.970 (0.59)	2.190 (0.39)	2.218 (0.42)
Mulliken charges			
Fe(1)	−0.04	+0.67	+0.60
N(2){pyridine}	+0.06	−0.04	−0.07
N(9){pyrazole}	+0.12	−0.06	−0.08
N(14){pyrazole}	+0.14	−0.07	−0.05
N(18){pyridine}	+0.06	−0.03	−0.07
N(25){pyrazole}	+0.11	−0.08	−0.08
N(30){pyrazole}	+0.22	−0.05	−0.05
Calculated (measured) $\chi_M T$ at 298 K/BM	—	3.8 (3.7)	3.3 (3.3)
Calculated (measured) D/cm^{-1}	—	30	3.0 (4.9)
Relative energy/kJ mol^{-1}	0	180	90

presumably due to the approximately non-bonding character of the t_{2g} orbitals. The large structural distortion evident in high-spin (C_2) $\mathbf{1}^{2+}$ is therefore unusual. This distortion is made up of two components: a twisting of the plane of one ligand relative to the other about the N{pyridine}–Fe–N{pyridine} vector (*i.e.* $\theta < 90°$, Scheme 1) and a motion of one ligand about the Fe ion, so that $\varphi < 180°$ (Scheme 1). These will now be considered in turn.

Twisting the plane of one L^1H ligand relative to the other lowers θ, reduces the symmetry from D_{2d} to D_2 and removes the degeneracy between the e-orbitals. This has two consequences for Fe–L^1H bonding. First, the antibonding interaction between the pyridine p_π orbitals and these two d-orbitals is reduced for one d function and increased for the other. The limit of this distortion has the two ligands coplanar with D_{2h} symmetry (*i.e.* $\theta = 0$). In this symmetry and with octahedral bite angles, the antibonding shifts are:

$$\varepsilon\,(b_2\{d_{xz}\}) = 0$$
$$\varepsilon\,(b_3\{d_{yz}\}) = 2e_\pi\,(\text{pyridine})$$

Distortion along this coordinate thus affords a $(b_2)^2(b_3)^1$ configuration and a reduced antibonding interaction between the metal d-electrons and the π-electrons on the ligand pyridine groups. Second, this same twist also leads to changes in the repulsive interaction of the e-orbitals with the pyrazole σ-lone pairs (see above). This repulsion is increased in the b_2 orbital, and decreased in the b_3 function, as θ is lowered, but is only present for $\alpha \neq 90°$. The importance of this additional antibonding interaction is clear from Fig. 6(a), which shows the variation in LFSE with decreasing twist angle. It is clear that the twist angle θ has a much greater influence on the LFSE when $\alpha = 73°$ than when $\alpha = 90°$. Hence, it would appear that the unusual Jahn–Teller distortion exhibited by $\mathbf{1[PF_6]_2}$ is favoured by the narrow bite angle of the L^1H ligand.

The second type of distortion, motion of one L^1H ligand about the Fe ion so that $\varphi < 180°$, has the effect of tilting the pyrazole lone pairs of that ligand away from one of the e-orbitals but of tilting the pyridine lone pair towards the other. This also leads to a net increase in the LFSE of the system [Fig. 6(b)]. Combining the two distortions, CLF calculations predict a gain in LFSE of *ca.* 400 cm^{-1} for the high-spin (C_2) isomer compared to the high-spin (D_{2d}) form, and that the room-temperature magnetic susceptibility $\chi_M T$ and zero-field splitting constant D will be smaller for the high-spin (C_2) isomer than for the high-spin (D_{2d}). The agreement between these latter parameters and the experimental values is excellent (Table 3).

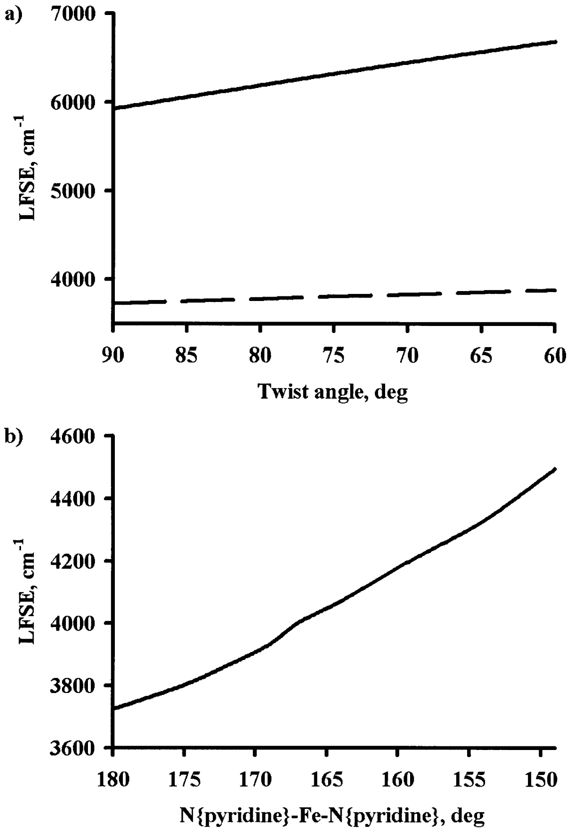

Fig. 6 (a) Calculated variation in LFSE of $\mathbf{1}^{2+}$ with increasing twist angle between the L^1H ligands (see text). The solid line refers to the experimentally observed ligand bite angle (α, Scheme 1) of 73°, whereas the dashed line refers to a model compound with $\alpha = 90°$. (b) Calculated variation of LFSE with N{pyridine}–Fe–N{pyridine} angle (Φ, Scheme 1).

Concluding remarks

This study emphasises that the solid state magnetic properties of $[Fe(L^1R)_2]^{2+}$ and similar Fe(II) compounds must be interpreted with care in the absence of structural data. A good illustration of this is $[Fe(L^4)_2][ClO_4]_2$, which is a spin-crossover complex in solution and can be crystallised in both high-spin and low-spin forms at 290 K.[23] However, solid high-spin $[Fe(L^4)_2][ClO_4]_2$ has a very distorted 'C_2' geometry, and is

Table 4 Experimental details for the new single crystal structure determinations in this study

	$[Fe(L^1H)_2][BF_4]_2\cdot2.9CH_3NO_2\cdot0.25H_2O$ (**1[BF$_4$]$_2$**$\cdot2.9CH_3NO_2\cdot0.25H_2O$)	$[Fe(L^1H)_2][PF_6]_2$ (**1[PF$_6$]$_2$**)
Formula	$C_{24.9}H_{27.2}B_2F_8FeN_{12.9}O_{6.05}$	$C_{22}H_{18}F_{12}FeN_{10}P_2$
M_r	833.43	768.25
Crystal class	Orthorhombic	Monoclinic
Space group	$P2_12_12_1$	$C2/c$
a/Å	13.8129(2)	14.2478(4)
b/Å	13.8303(1)	9.4974(3)
c/Å	36.4266(4)	20.5607(5)
β/°	—	99.3180(19)
U/Å^3	6958.81(14)	2745.50(13)
Z	8	4
μ(Mo-Kα)/mm^{-1}	0.538	0.761
T/K	150(2)	120(2)
Measured reflections	65933	10414
Independent reflections	15894	3141
R_{int}	0.070	0.049
$R(F)^a$	0.051	0.034
$wR(F^2)^b$	0.162	0.090
S	1.100	1.045
Flack parameter	−0.006(12)	—

[a] $R = \Sigma[|F_o| - |F_c|]/\Sigma|F_o|$. [b] $wR = [\Sigma w(F_o^2 - F_c^2)/\Sigma wF_o^4]^{1/2}$.

high-spin between 4 and 290 K. Hence, solution data are a better guide to the ligand field experienced by an Fe(II) complex than its solid state magnetic properties. This is because the lability of high-spin Fe(II) centres would allow the rapid interconversion of the D_{2d} and C_2 isomers of these compounds in solution.

There are inconsistencies in the magnetochemistry of different salts of other $[FeL_2]^{2+}$ (L = a meridional tridentate imine) complexes in the solid state and/or solution, in addition to the terpyridyl derivatives in the previous paragraph. Examples we are aware of include: $[Fe(L^5H)_2]Cl_2$ which is a spin-crossover complex, whereas salts of $[Fe(L^5Me)_2]^{2+}$ are high-spin over the entire temperature range, even though the latter compound experiences a slightly greater ligand field;[26] different solid salts of $[Fe(L^6Me)_2]^{2+}$ which are either low-spin or high-spin in the range 10–330 K;[27] and the spin-crossover complex $[Fe(L^6H)_2][BPh_4]_2\cdot4H_2O$ which reverts to a high-spin form upon dehydration.[28] Differences in lattice hydrogen bonding may account for many of these observations.[7] However, this work has suggested an alternative explanation: that the high-spin forms of these solid compounds are 'trapped' as a C_2-symmetric isomer, which is unable to undergo spin-crossover. This is particularly relevant to the above compounds, since our calculations show that the C_2 form is stabilised by the use of constrained chelating ligands with acute bite angles.

Experimental

Unless stated otherwise, all manipulations were performed in air using commercial grade solvents. 2,6-Di(pyrazol-1-yl)pyridine (L^1H)[13] was prepared by the literature procedures. $FeCl_2$ (Avocado), $Fe[BF_4]_2\cdot6H_2O$ and NH_4PF_6 (Aldrich) were used as supplied.

Syntheses

Synthesis of $[Fe(L^1H)_2][BF_4]_2$ (1[BF$_4$]$_2$). A solution of $Fe[BF_4]_2\cdot6H_2O$ (0.20 g, 5.92×10^{-4} mol) and L^1H (0.25 g, 1.18×10^{-3} mol) in acetone (50 cm^3) was stirred at room temperature for 15 min. The resultant brown solution was filtered and concentrated to *ca.* 1/3 of its original volume, whereupon a mustard-coloured precipitate formed. Following overnight storage at −30 °C, the product was filtered and washed sequentially with cold MeOH and Et_2O. Recrystallisation from $MeNO_2/Et_2O$ yielded golden platelets. Yield 0.24 g, 62% (Found: C, 40.7; H, 2.0; N, 22.0. Calc. for $C_{22}H_{18}B_2F_8FeN_{10}$: C, 40.5; H, 2.8; N, 21.5%). FAB MS: *m/z* 478 $[^{56}Fe(L^1H)_2]^+$, 266 $[^{56}Fe(L^1H–H]^+$. ^1H NMR sepectrum (CD_3CN, 298 K): δ 61.7, 56.9, 36.6, 34.6 (all 4H, Py $H^{3/5}$ + Pz H^3–H^5), 2.6 (2H, Py H^4) ppm. UV/vis spectrum (MeCN, 298 K): $\nu_{max}/10^3$ cm^{-1} (ε_{max}/M^{-1} cm^{-1}) 9.7 (8.4), 11.1 (sh), 23.9 (1400), 26.3 (sh), 33.3 (41300), 37.5 (39800), 40.9 (69000), 41.8 (54000), 47.2 (17300). UV/vis spectrum ($MeNO_2$, 298 K): $\nu_{max}/10^3$ cm^{-1} (ε_{max}/M^{-1} cm^{-1}) 9.6 (8.6), 11.1 (sh), 23.8 (2000), 25.6 (1900).

Synthesis of $[Fe(L^1H)_2][PF_6]_2$ (1[PF$_6$]$_2$). A mixture of $FeCl_2\cdot4H_2O$ (0.12 g, 5.92×10^{-4} mol) and L^1H (0.25 g, 1.18×10^{-3} mol) was refluxed in MeOH (25 cm^3) until all of the solid had dissolved (*ca.* 1 h). After addition of NH_4PF_6 (0.19 g, 1.18×10^{-3} mol), the deep yellow solution was refluxed for a further 15 min. The hot solution was filtered, cooled and concentrated to approximately half volume, whereupon a yellow solid began to precipitate. Following overnight storage at −30 °C, the product was filtered and washed sequentially with MeOH and Et_2O. Recrystallisation from acetone/Et_2O afforded yellow microcrystals. Yield 0.33 g, 73% (Found: C, 34.5; H, 2.3; N, 18.2. Calc. for $C_{22}H_{18}F_{12}FeP_2F_{10}$: C, 34.4; H, 2.4; N, 18.2%).

Single crystal X-ray structure determinations

Single crystals of X-ray quality of **1[BF$_4$]$_2$** and **1[PF$_6$]$_2$** and were grown by diffusion of diethyl ether vapour into solutions of the complexes in acetone at 290 K. Single crystals of **1[BF$_4$]$_2$**$\cdot2.9CH_3NO_2\cdot0.25H_2O$ were obtained by slow diffusion of Et_2O into a $MeNO_2$ solution of the complex at 240 K; these crystals were cooled over solid CO_2 during mounting, to avoid decomposition. Full details of the structure determinations of **1[BF$_4$]$_2$** have been published previously.[11] Experimental details for the other structure determinations are given in Table 4. All structures were solved by direct methods (SHELXS 97)[29] and refined by full matrix least-squares on F^2 (SHELXL 97)[30] with H atoms placed in calculated positions.

CCDC reference numbers 171144 and 171145.

See http://www.rsc.org/suppdata/dt/b1/b108468m/ for crystallographic data in CIF or other electronic format.

X-Ray structure determination of $[Fe(L^1H)_2][BF_4]_2\cdot2.9CH_3NO_2\cdot0.25H_2O$ (1[BF$_4$]$_2$$\cdot$2.9CH$_3NO_2$$\cdot$0.25H$_2$O). The asymmetric unit contains two complex cations, four anions, six CH_3NO_2 molecules and one feature that was not bonded to any other atom, and was modelled as half a molecule of water. The F atoms of one of the BF_4^- anions were disordered over three orientations in a 0.5 : 0.3 : 0.2 occupancy ratio. Another BF_4^- moiety was modelled over two orientations in a

0.6 : 0.4 occupancy ratio. All B–F bonds within the disordered anions were restrained to 1.38(2) Å, and the corresponding non-bonded F ⋯ F contacts within a given disorder orientation to 2.25(2) Å. Four of the CH_3NO_2 molecules were wholly occupied and ordered; one was wholly occupied but disordered over two orientations in a 0.6 : 0.4 occupancy ratio; and one had a total occupancy of 0.8, spread between two equally occupied orientations with a central shared N atom. All non-H atoms with an occupancy ≥0.5 were refined anisotropically.

X-Ray structure determinations of $[Fe(L^1H)_2][PF_6]_2$ ($1[PF_6]_2$). During refinement, the F atoms of the PF_6^- anion were found to be disordered over two equally occupied orientations. All P–F bonds were restrained to 1.60(2) Å during the final least-squares cycles, and all non-H atoms were modelled anisotropically.

Other measurements

Infra-red spectra were obtained as Nujol mulls pressed between KBr windows over 400–4000 cm^{-1} using a Nicolet Avatar 360 spectrophotometer. UV/visible spectra were obtained with a Perkin-Elmer Lambda 900 spectrophotometer operating over 3300–200 nm, using 1 cm quartz cells. All ^1H NMR spectra were run on a Bruker DPX250 spectrometer, operating at 250.1 MHz. Positive ion fast atom bombardment mass spectra were performed on a Kratos MS50 spectrometer, employing a 3-NOBA matrix. CHN microanalyses were performed by the University of Leeds School of Chemistry microanalytical service.

Room-temperature magnetic moments were measured using a Sherwood Scientific susceptibility balance. Variable temperature magnetic susceptibility measurements were obtained in the solid state using a Quantum Design SQUID magnetometer operating at 1000 G. Diamagnetic corrections for the sample and the sample holder were applied. Observed and calculated data were refined using SIGMAPLOT.[31] Magnetic susceptibility measurements in solution were obtained by Evans's method[32] using a Bruker DRX500 spectrometer operating at 500.13 MHz. A diamagnetic correction for the sample was applied to these data. Diamagnetic corrections were estimated from Pascal's constants.[14]

All density functional (DF) calculations were performed using the 'DeFT' code written by St-Amant[33] in the linear combination of Gaussian-type orbitals framework. Calculations were performed using the Vosko–Wilk–Nusair[34] local spin density approximation of the correlation part of the exchange-correlation potential, with non-local corrections using the Becke functional for exchange[35] and the Perdew functional for correlation.[36] The all-electron calculations used triple-ζ basis sets for all the elements except iron, for which basis functions of double-ζ quality were used. Bond orders were calculated according to the prescription suggested by Mayer.[37] Cellular ligand field calculations[38,39] were performed using the parameters e_σ (pyridine) = 6100 cm^{-1}, e_σ (pyrazole) = 4400 cm^{-1} and $e_{\pi\perp} = 0.25e_\sigma$, to characterise the σ-donor strength and any π-bonding perpendicular to the plane of the nitrogen ligands. The parameters B = 550 cm^{-1}, ζ = 400 cm^{-1} and the orbital reduction factor $k = 0.8$ were also employed.

Acknowledgements

The Royal Society (M. A. H., J. M. H.), the EPSRC, the University of Leeds and the University of Hull are acknowledged for financial support.

References

1 N. K. Solanki, E. J. L. McInnes, F. E. Mabbs, S. Radojevic, M. McPartlin, N. Feeder, J. E. Davies and M. A. Halcrow, *Angew. Chem., Int. Ed. Engl.*, 1998, **37**, 2221.
2 A. J. Bridgeman, M. A. Halcrow, M. Jones, E. Krausz and N. K. Solanki, *Chem. Phys. Lett.*, 1999, **314**, 176.
3 M. A. Leech, N. K. Solanki, M. A. Halcrow, J. A. K. Howard and S. Dahaoui, *Chem. Commun.*, 1999, 2245.
4 N. K. Solanki, M. A. Leech, E. J. L. McInnes, J. P. Zhao, F. E. Mabbs, N. Feeder, J. A. K. Howard, J. E. Davies, J. M. Rawson and M. A. Halcrow, *J. Chem. Soc., Dalton Trans.*, 2001, 2083.
5 J. M. Holland, C. A. Kilner, M. Thornton-Pett and M. A. Halcrow, *Polyhedron*, 2001, **20**, 2829.
6 E. König, *Prog. Inorg. Chem.*, 1987, **35**, 527.
7 P. Gütlich, A. Hauser and H. Spiering, *Angew. Chem., Int. Ed. Engl.*, 1994, **33**, 2024.
8 K. H. Sugiyarto and H. A. Goodwin, *Aust. J. Chem.*, 1988, **41**, 1645.
9 K. H. Sugiyarto, D. C. Craig, A. D. Rae and H. A. Goodwin, *Aust. J. Chem.*, 1994, **47**, 869; K. H. Sugiyarto, K. Weitzner, D. C. Craig and H. A. Goodwin, *Aust. J. Chem.*, 1997, **50**, 869; K. H. Sugiyarto, M. L. Scudder, D. C. Craig and H. A. Goodwin, *Aust. J. Chem.*, 2000, **53**, 755.
10 H. A. Goodwin and K. H. Sugiyarto, *Chem. Phys. Lett.*, 1987, **139**, 470; E. König, B. Kanellakopulos, B. Powietzka and H. A. Goodwin, *Inorg. Chem.*, 1989, **28**, 3993; T. Buchen, P. Gütlich and H. A. Goodwin, *Inorg. Chem.*, 1994, **33**, 4573; T. Buchen, P. Gütlich, K. H. Sugiyarto and H. A. Goodwin, *Chem. Eur. J.*, 1996, **2**, 1134; R. Lubbers, G. Nowietzke, H. A. Goodwin and G. Wortmann, *J. Phys. IV*, 1997, **7**, 651.
11 J. M. Holland, J. A. McAllister, Z. Lu, C. A. Kilner, M. Thornton-Pett and M. A. Halcrow, *Chem. Commun.*, 2001, 577.
12 T. Ayers, S. Scott, J. Goins, N. Caylor, D. Hathcock, S. J. Slattery and D. L. Jameson, *Inorg. Chim. Acta*, 2000, **307**, 7.
13 D. L. Jameson and K. A. Goldsby, *J. Org. Chem.*, 1990, **55**, 4992.
14 C. J. O'Connor, *Prog. Inorg. Chem.*, 1982, **29**, 203.
15 D. W. Blakesley, S. C. Payne and K. S. Hagen, *Inorg. Chem.*, 2000, **39**, 1979.
16 P. W. Atkins, *Physical Chemistry*, Oxford University Press, Oxford, 2nd edn., 1982, pp. 267–269.
17 A. B. P. Lever, *Inorganic Electronic Spectroscopy*, Elsevier, Amsterdam, 2nd edn., 1984, pp. 458–470.
18 M. Mikami, M. Konno and Y. Saito, *Chem. Phys. Lett.*, 1979, **63**, 566.
19 P. Guionneau, J.-F. Létard, D. S. Yufit, D. Chasseau, G. Bravic, A. E. Goeta, J. A. K. Howard and O. Kahn, *J. Mater. Chem.*, 1999, **9**, 985.
20 Y. Garcia, P. Guionneau, G. Bravic, D. Chasseau, J. A. K. Howard, O. Kahn, V. Ksefontov, S. Reiman and P. Gütlich, *Eur. J. Inorg. Chem.*, 2000, 1531.
21 A. F. Stassen, M. de Vos, P. J. van Koningsbruggen, F. Renz, J. Ensling, H. Kooijman, A. L. Spek, J. G. Haasnoot, P. Gütlich and J. Reedijk, *Eur. J. Inorg. Chem.*, 2000, 2231.
22 G. S. Matouzenko, A. Bousseksou, S. Lecocq, P. J. van Koningsbruggen, M. Perrin, O. Kahn and A. Collet, *Inorg. Chem.*, 1997, **36**, 5869.
23 E. C. Constable, G. Baum, E. Bill, R. Dyson, R. van Eldik, D. Fenske, S. Kaderli, D. Morris, A. Neubrand, M. Neuberger, D. R. Smith, K. Wieghardt, M. Zehnder and A. D. Zuberbühler, *Chem. Eur. J.*, 1999, **5**, 498.
24 G. Chen, C. Espinosa-Perez, A. Zentella-Dehesa, I. Silaghi-Dumitrescu and F. Lara-Ochoa, *Inorg. Chem.*, 2000, **39**, 3440.
25 H. Paulsen, L. Duelund, H. Winkler, H. Toftlund and A. X. Trautwein, *Inorg. Chem.*, 2001, **40**, 2201.
26 K. H. Sugiyarto, D. C. Craig, A. D. Rae and H. A. Goodwin, *Aust. J. Chem.*, 1993, **46**, 1269.
27 A. W. Addison, S. Burman, C. G. Wahlgren, O. A. Rajan, T. M. Rowe and E. Sinn, *J. Chem. Soc., Dalton Trans.*, 1987, 2621.
28 R. Boca, P. Baran, M. Boca, L. Dhlán, H. Fuess, W. Haase, W. Linert, B. Papánková and R. Werner, *Inorg. Chim. Acta*, 1998, **278**, 190.
29 G. M. Sheldrick, *Acta Crystallogr., Sect. A*, 1990, **46**, 467.
30 G. M. Sheldrick, SHELXL 97, Program for the Refinement of Crystal Structures, University of Göttingen, Germany, 1997.
31 SIGMAPLOT, Program for Tabulating, Modelling and Displaying Data (v. 5.0), SPSS Inc., Chicago, IL, 1999.
32 D. F. Evans, *J. Chem. Soc.*, 1959, 2003; E. M. Schubert, *J. Chem. Educ.*, 1992, **69**, 62.
33 A. St-Amant, DeFT, a Fortran program, University of Ottawa, Canada, 1994.
34 S. H. Vosko, L. Wilk and M. Nusair, *Can. J. Phys.*, 1980, **58**, 1200.
35 A. D. Becke, *Phys. Rev. A*, 1988, **38**, 3098.
36 J. P. Perdew, *Phys. Rev. B*, 1986, **33**, 8822.
37 I. Mayer, *Int. J. Quantum Chem.*, 1984, **26**, 151.
38 A. J. Bridgeman and M. Gerloch, *Prog. Inorg. Chem.*, 1996, **45**, 179.
39 A. R. Dale, M. J. Duer, N. D. Fenton, M. Gerloch and R. F. McMeeking, CAMMAG4, a Fortran program, University of Cambridge, Cambridge, 1994.